Nonponderomotive electron acceleration in ultrashort surface-plasmon fields

Péter Rácz and Péter Dombi
Wigner Research Centre for Physics, Konkoly-Thege M. út 29-33, H-1121 Budapest, Hungary
(Received 1 September 2011; published 22 December 2011)

We investigate the nonponderomotive nature of ultrafast plasmonic electron acceleration in strongly decaying electromagnetic fields generated by few-cycle and single-cycle femtosecond laser pulses. We clearly identify the conditions contributing to nonponderomotive acceleration and establish fundamental scaling laws and carrier-envelope phase effects. These all-optically accelerated compact, femtosecond electron sources can be utilized in contemporary ultrafast methods.

DOI: 10.1103/PhysRevA.84.063844 PACS number(s): 42.65.Re, 73.20.Mf, 41.75.Jv

I. INTRODUCTION

It is known that an electromagnetic wave with a spatially inhomogeneous amplitude distribution (such as, for example, a focused Gaussian laser pulse) can accelerate electrons with the so-called ponderomotive acceleration mechanism upon subsequent optical cycles (see Refs. [1–5] and references therein). This phenomenon was exploited in the vicinity of metal surfaces to generate ultrashort electron bunches with up to keV energy by drawing on ultrafast surface-plasmon excitations [6–9]. In a parallel development, rapid advances in femtosecond laser technology enabled the temporal duration of laser pulses to break through the few-cycle [10,11] and, more recently, the single-cycle [12,13] barriers. These pulses, when focused, represent wavelength-scale "light bullets" according to their spatial dimensions. They can be further confined to subwavelength spatial scales to metal surfaces [as surface-plasmon polaritons (SPPs)] [9] or nanostructures [as localized plasmons (LPs)] [14]. The resulting highly localized electromagnetic fields can accelerate photoelectrons all optically to several keV on subwavelength distances [8,9,15]. The fact that the electron injection into the accelerating field is facilitated by the same laser pulse makes an ultrafast and ultracompact acceleration scheme possible.

If laser pulses are "long" (i.e., made up of several optical cycles), and the field amplitude changes "slowly" in space (i.e., compared to the wavelength) the ponderomotive electron acceleration process is governed by the so-called ponderomotive potential given by

$$U_p = \frac{e^2\lambda^2 E^2}{16\pi^2 m_e c^2}, \tag{1}$$

where e is the electron charge, m_e is the electron mass, λ, E, and c are the wavelength, field strength amplitude, and speed of the light, respectively. It can be shown that if the field amplitude of an electromagnetic wave packet has a gradient in any direction, free electrons placed in this field will be accelerated along the gradient of the ponderomotive potential. This is enabled by the differing field amplitudes the electron experiences upon subsequent cycles of its trip in the electric field, thereby experiencing a cycle-by-cycle acceleration.

Here, we show that this ponderomotive picture of the electron gaining kinetic energy cyce-by-cycle breaks down (a) when it comes to electron acceleration in few-cycle or single-cycle optical wave packets, or (b) when the (plasmonic) field decays rapidly within some hundreds of nm on a distance comparable to the wavelength. Thus, investigation of ponderomotive versus nonponderomotive features of the acceleration process becomes highly important in order to enable full optical field control of the properties of the electron bunch. Therefore, we model and investigate ultrafast plasmonic, nonponderomotive electron acceleration in a general manner in SPP fields. We clearly identify the phenomena contributing to nonponderomotive effects. In addition, we establish fundamental wavelength and intensity scaling laws of the process. These results can be easily applied and generalized for tailoring ultrafast electron sources in any configuration where steeply changing ultrashort fields are involved, such as plasmonic [9,14] and tip-enhanced [16,17] ultrafast photoemission or electron generation from isolated dielectric nanoemitters [18].

II. MODEL

For a deeper understanding of the scaling of the plasmonic photoemission and electron acceleration process, we used a simulation method based on a three-step model [19]. This model can be summarized as a sequence of three distinct events: (i) The coupling of the laser field to the SPP propagating at the metal surface (in Kretschmann configuration), building up an evanescent plasmonic field. (ii) Then, photoelectron emission is induced by this SPP field. The photoemission is of multiphoton or tunneling type depending on the intensity. (iii) Finally, free electrons are accelerated in the nanometer scale evanescent surface-plasmon field at the vacuum side of the metal layer. Figure 1(a) illustrates this process. For the actual modeling, the temporal evolution and spatial distribution of the SPP field was described first by an analytic formula [19], instead of the computationally intensive numerical solution of Maxwell's equations in the Kretschmann SPP coupling configuration [20]. It was shown that results of our model can reproduce very well the results based on the exact solution of Maxwell's equations [21]. In the second step, the temporal and spatial emission profiles were determined by the Fowler-Nordheim equation at different points of the surface. This equation can be used to determine the instantaneous tunneling current in this intensity regime [22]. (For the application of this formula we took into consideration a 15× enhancement factor of the SPP field relative to the laser field, agreeing well with experimental results [9]). Finally, the equations of motion of thousands of electrons were

numerically solved in the evanescent SPP field starting from different initial positions along the surface and for different photoemission instants. Some of these calculated electron trajectories can be seen in Fig. 1(a) (blue/light gray curves). A portion of these trajectories show that some electrons return to the metal surface after free motion in vacuum. When this happens, reabsorption of the electrons was assumed in this calculation, since this simplified model cannot capture the exact recollision process. Processes such as rescattering, recombination, and high-order harmonic generation analogous to atomic recollision phenomena [23,24] also take place, as it was demonstrated in a recent experiment involving sharp metal tips [25]. An above threshold photoemission, however, does not influence the spectrum of the plasmonically accelerated electron beam substantially, as it decays rapidly within a range of a few times the photon energy [25]. Therefore, after applying appropriate statistics to a large number of trajectories calculated in the manner described above, one can determine the measurable spectrum of the ultrafast electron bunch with a very good approximation. This is also supported by the agreement of experimentally measured and reconstructed electron spectra for this particular configuration [8,9,15].

III. MODEL RESULTS

Figure 1(b) illustrates three typical calculated electron spectra at different maximal field strengths on a logarithmic scale. The maximum field strengths were determined taking plasmonic field enhancement also into account (15×), which results in a 225× enhancement of the ponderomotive potential according to Eq. (1). A Gaussian pulse with a 5-fs full width at half maximum pulse length at an 800-nm wavelength with a $\varphi_0 = 0$ carrier-envelope phase (CEP) was assumed in this computation. As opposed to our previous numerical results [19], we assumed a 0-attosecond (as) tunneling time delay in this particular computation, as very recent experimental and theoretical evidence in this rapidly evolving field of research also points toward this working hypothesis [26–29]. The actual value of the tunneling time delay, however, does not influence the conclusions to be drawn in this paper in any way whatsoever. The reason is that this value influences the actual shape of the spectra but it does not affect the cutoff positions. We will illustrate nonponderomotive features by investigating the cutoffs.

Characteristically, Fig. 1(b) shows low-energy peaks in the spectra and sharp cutoffs appear at higher energy after a strong decay of the count rate. The positions of the peaks and cutoffs depend on the maximum plasmonic field strength. These observations are in accordance with recent experiments [9]. By further analyzing spectra similar to those in Fig. 1(b), interesting observations can be made. In Fig. 2(a), the scaling of the cutoff positions in the electron spectra are depicted as a function of peak plasmonic field strength ($E_{\max}$) for two pulse lengths (for few-cycle 5-fs pulses and for multicycle 50-fs pulses). The other parameters of this computation are the same as for those in Fig. 1(b). Deviations from the ponderomotive scaling are obvious. For example, in the 50-fs case, the exponent of the best-fit curve is 2.214 (±0.005), therefore, the electron energy cutoff dependence is stronger than linear with respect to the intensity. We begin by discussing this result. Because of the fact that the decay of the SPP field takes place in a distance (∼660 nm) comparable to the wavelength, the electrons do not experience an incremental kinetic energy gain in subsequent field oscillation cycles (which is an inherent ansatz for the ponderomotive potential picture) provided that the field strengths are high. With these parameters, the field amplitude can change significantly even within one oscillation cycle along the electron trajectory, and this effect is obviously stronger for higher-field strengths due to the longer trajectories involved. Exactly this provides the superponderomotive scaling observed in this case. This effect is illustrated in Figs. 2(b)–2(d), where electron trajectories are depicted for illustration for 5- and 50-fs input pulses and different field strengths for comparison. Figure 2(e) shows the decay of the field on the same scale. For example, by

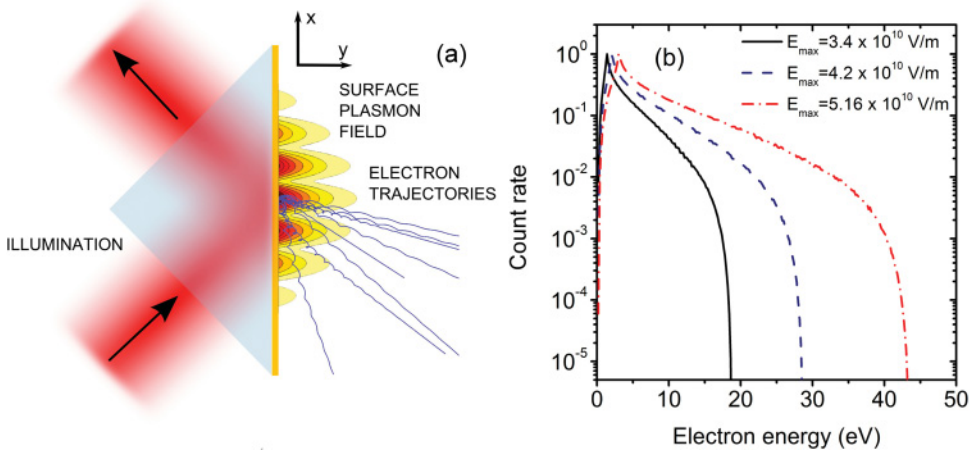

FIG. 1. (Color online) (a) Illustration of electron generation and acceleration by surface plasmons in the Kretschmann coupling configuration. The electric field amplitude distribution at the vacuum side of the thin metal film is shown with the contour plot; some representative electron trajectories are shown in blue (light gray). (b) Typical computed SPP accelerated electron spectra at different maximal field strengths for a cosinelike Gaussian laser pulse with a 5-fs pulse length (intensity full width at half maximum) and an 800-nm central wavelength.

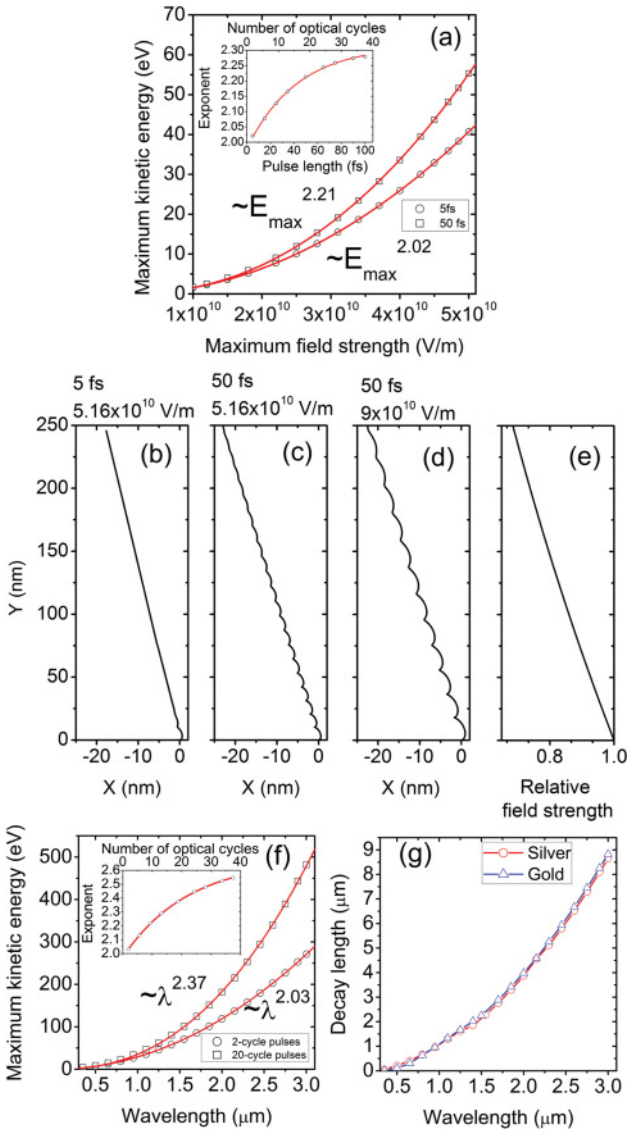

FIG. 2. (Color online) (a) The maximum kinetic energy of plasmonically accelerated electrons as a function of maximum electric field strength for different pulse lengths and a central wavelength of 800 nm. Circles represent results for 5-fs pulses, and squares are for 50-fs pulses. Solid lines are exponential fits to these curves with the exponent as a fit parameter. The inset shows the exponent of the fitting as a function of pulse duration. (b),(c) Sample calculated electron trajectories with 5- and 50-fs pulse lengths ($\varphi_0 = 0$) and 5.16×10^{10} V/m maximum field strength. (d) Sample calculated electron trajectory with a 50-fs pulse length and 9×10^{10} V/m maximum field strength. (e) Normalized decay of the plasmonic field in vacuum as a function of the distance from the surface. (f) The maximum kinetic energy of plasmonically accelerated electrons as a function of wavelength and exponential fits to these curves (solid lines). Circles represent the ∼2 optical cycle case (5 fs at 800 nm), and squares represent the ∼20 optical cycle case (50 fs at 800 nm). The inset shows the exponent of the fitting as a function of the number of optical cycles. (g) The vacuum decay length of surface-plasmon fields at different wavelengths for silver and gold films.

comparing Figs. 2(c) and 2(d), longer trajectories in the inhomogeneous field for higher-field strengths are clearly visible.

In contrast, the field scaling exponent is 2.023 (±0.001) for 5-fs input pulse lengths. This is closer to the ponderomotive scaling value for the following reason. In the short-pulse limit, the few-cycle plasmonic wave packet [9] passes in time so quickly that the electrons cannot cover the distance of the decay length (which is 661 nm at this wavelength), and therefore the acceleration for such short pulses occurs in an almost homogeneous field. For longer pulse lengths, more and more of the decaying field is "utilized" for the acceleration of the electron. However, this is also limited as soon as the electron approaches a distance from the surface comparable to the decay length of the SPP field. Here, the "saturation" of the scale exponent is observed taking place for >100-fs pulse lengths. This is illustrated by the pulse length dependence of the scale exponent in the inset of Fig. 2(a). Therefore, we can state that for this particular plasmonic decay length a superponderomotive scaling of the maximum electron energy with $E_{\max}^{2.3}$ is observed.

We investigated also the wavelength scaling of the acceleration process. The results of this simulation are presented in Fig. 2(f). The maximum plasmonic field strength was 3.4×10^{10} V/m, and the pulse length corresponded to the same number of optical cycles each time (∼2, which corresponds to a 5-fs pulse length at 800 nm and 15 fs at 2400 nm). For comparison, results for 20-cycle pulses are also plotted. The CEP value was assumed to be $\varphi_0 = 0$. The wavelength dependence of the decay length [Fig. 2(g)] also was taken into consideration. It was calculated analytically in the case of silver and gold by the formula $z(\lambda) = \frac{\lambda}{2\pi}\sqrt{\frac{\varepsilon_1(\lambda)+\varepsilon_0}{\varepsilon_0^2}}$ [30], where ε_1 is the dielectric constant of the metal and ε_0 is the dielectric constant of vacuum. The value of the dielectric coefficient of the metals was taken from Ref. [31].

It can be seen again in Fig. 2(f) that, for longer pulses, the maximum kinetic energies scale in a superponderomotive manner with the wavelength, whereas exponents closer to 2 are observed for shorter pulses. The inset of Fig. 2(f) depicts the exponent of the fitting as a function of the number of optical cycles of the pulse. The arguments and the discussion presented above are also applicable here. The longer is the wavelength, the more distance the electrons reach away from the surface during the acceleration process, where the field decay becomes significant. Therefore, the wavelength difference has a similar effect on the scale exponent as the intensity difference, which is also easily seen from Eq. (1). This demonstrates another aspect of nonponderomotive acceleration.

We also argue that the electron acceleration process is nonponderomotive even in the few-cycle case, even though the scale exponent is much closer to the value expected from classical ponderomotive processes. We support this statement with the following study. We calculated and plotted the carrier-envelope phase (CEP) dependence of the cutoff electron energy as a function of the pulse length, which is shown in Fig 3(a) in a false color representation. In this calculation the maximum SPP field strength was 3.4×10^{10} V/m again, and an 800-nm central wavelength was assumed. Four lineouts are also plotted in Fig. 3(b) for a better illustration of the CEP sensitivity of the process. In the few-cycle regime, the maximum kinetic energy even has a 50% CEP modulation which is continuously decreasing toward longer pulse lengths. The reason of this

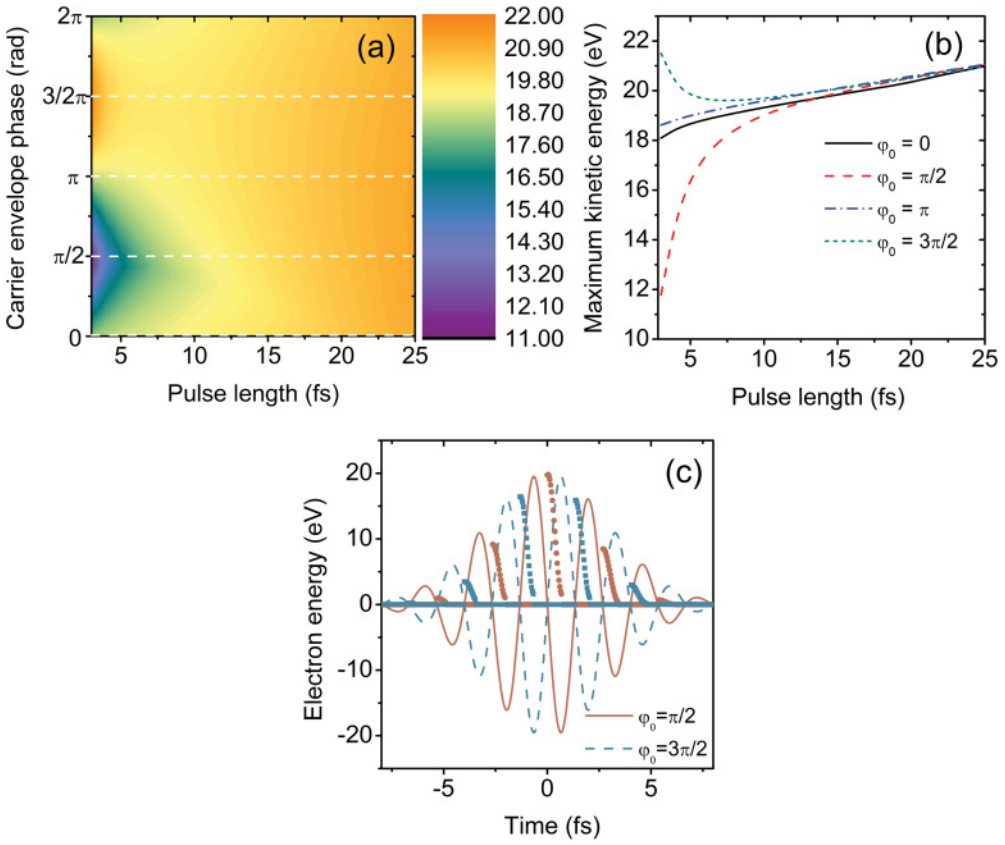

FIG. 3. (Color online) (a) The maximum kinetic energy of plasmonically accelerated electrons as a function of pulse duration and the carrier-envelope phase (CEP, φ_0) of the pulses. Lineouts at the dashed line are depicted in (b) at four different CEP values. (c) The final kinetic energy of the electrons as a function of the emission instant of the electrons at two different CEPs (brown circles represent $\varphi_0 = \pi/2$ and blue squares represent $\varphi_0 = 3\pi/2$) as well as the waveforms of the plasmon generating 5-fs laser pulses (brown solid line for $\varphi_0 = \pi/2$ and blue dashed line for $\varphi_0 = 3\pi/2$). See text for further details.

relatively high contrast between cutoffs for different CEP values is that in the few-cycle regime the final kinetic energies of the electrons emitted at different time instants along the SPP pulse can differ significantly depending on the actual CEP of the pulse. This is illustrated in Fig 3(c), where the final kinetic energy was depicted as a function of the emission instant of electrons with a 5-fs pulse length and at $\varphi_0 = \pi/2$ (circles) and $\varphi_0 = 3\pi/2$ CEP (squares) values. We also plotted the field strength evolution of both pulses for reference.

Based on this illustration, the few-cycle region is nonponderomotive from two aspects. The electrons do not have time to see the ponderomotive force character of the oscillating surface-plasmon field due to the extremely short duration of the plasmonic wave packet. Although the scaling of the cutoff with a maximum field strength gives back the quadratic scaling value [see Fig. 2(a)], the usual time average of the field defining the ponderomotive potential is not usable here, which is also shown by the high CEP dependence of the maximum kinetic energy. Therefore, pulses with exactly the same envelope and spatial intensity distribution result in completely different electron spectra signifying the breakdown of the ponderomotive acceleration picture. It can also be seen according to Fig. 3(b) that this breakdown takes place for pulses with a less than ∼12-fs pulse duration corresponding to four to five optical cycles at an 800-nm central wavelength. For longer pulses than this, nonponderomotive effects also do arise in this particular plasmonic electron acceleration scheme, but they are rooted in the strongly decaying SPP field in the vicinity of the surface.

IV. SUMMARY

One can sum up the observed nonponderomotive effects in ultrafast plasmonic fields in the following way. If the temporal or spatial intensity distribution of a laser pulse is such that these intensity changes take place on a scale comparable to the carrier wavelength, nonponderomotive electron acceleration effects take place in these highly confined, high-intensity fields. This has to be considered in order to be able to understand ultrafast plasmonic electron acceleration [6–9] and other strong-field phenomena [16–18] in the case of either extreme spatial or temporal electromagnetic field confinement.

In order to be able to further improve ultrafast methods, the development of state-of-the-art, ultrafast electron emitters are of utmost importance. The electron source is known to determine the ultimate performance and resolution of these devices and, therefore, investigations on the fundamentals of ultrafast electron emission and all-optical acceleration can bring significant advances in these fields. By a detailed investigation of ultrafast plasmonic electron acceleration (such

as the scaling of the maximal kinetic energy of the electrons as a function of maximal field strength, the wavelength, and the CEP dependence), we found nonponderomotive features in the observable electron spectra both in the multicycle and in the few-cycle regimes of pulse duration. These nonponderomotive effects are rooted either in the fast spatial decay of SPP fields or in the few-cycle nature of the pulses. However, both phenomena correspond to the fact that these fields are highly confined, thus signifying a different regime of ultrafast light-matter interactions than those described previously. These findings are also important for contemporary high-harmonic-generation schemes [32,33] and for tip-based nanoemitters [16,17,22,25] where the trajectory of the electrons traverses a localized electric field with a highly inhomogeneous amplitude distribution.

ACKNOWLEDGMENTS

The authors acknowledge support from the Hungarian Scientific Research Fund (OTKA project 81364). P.D. was supported by the János Bolyai Research Scholarship of the Hungarian Academy of Sciences.

[1] H. Boot and R. Harvie, Nature (London) **180**, 1187 (1957).
[2] A. V. Gaponov and M. A. Miller, Sov. Phys. JETP **7**, 168 (1958).
[3] J. Kupersztych, Phys. Rev. Lett. **54**, 1385 (1985).
[4] A. E. Kaplan and A. L. Pokrovsky, Phys. Rev. Lett. **95**, 053601 (2005).
[5] D. Lin, Q. Kong, Z. Chen, P. X. Wang, and Y. K. Ho, J. Phys. D **41**, 135107 (2008).
[6] J. Kupersztych, P. Monchicourt, and M. Raynaud, Phys. Rev. Lett. **86**, 5180 (2001).
[7] J. Zawadzka, D. Jaroszynski, J. J. Carey, and K. Wynne, Appl. Phys. Lett. **79**, 2130 (2001).
[8] S. E. Irvine, A. Dechant, and A. Y. Elezzabi, Phys. Rev. Lett. **93**, 184801 (2004).
[9] P. Dombi *et al.*, Opt. Express **18**, 24206 (2010).
[10] V. S. Yakovlev, P. Dombi, G. Tempea, C. Lemell, J. Burgdörfer, T. Udem, and A. Apolonski, Appl. Phys. B **76**, 329 (2003).
[11] P. Dombi, V. S. Yakovlev, K. O'Keeffe, T. Fuji, M. Lezius, and G. Tempea, Opt. Express **13**, 10888 (2005), and references therein.
[12] G. Krauss, S. Lohss, T. Hanke, A. Sell, S. Eggert, R. Huber, and A. Leitenstorfer, Nat. Photonics **4**, 33 (2010).
[13] A. Wirth *et al.*, Science **334**, 195 (2011).
[14] A. Kubo, K. Onda, H. Petek, Z. Sun, Y. S. Jung, and H. K. Kim, Nano Lett. **5**, 1123 (2005).
[15] P. Rácz, S. E. Irvine, M. Lenner, A. Mitrofanov, A. Baltuška, A. Y. Elezzabi, and P. Dombi, Appl. Phys. Lett. **98**, 111116 (2011).
[16] R. Bormann, M. Gulde, A. Weismann, S. V. Yalunin, and C. Ropers, Phys. Rev. Lett. **105**, 147601 (2010).
[17] M. Krüger, M. Schenk, and P. Hommelhoff, Nature (London) **475**, 78 (2011).
[18] S. Zherebtsov *et al.*, Nat. Phys. **7**, 656 (2011).
[19] P. Dombi and P. Rácz, Opt. Express **16**, 2887 (2008).
[20] S. E. Irvine and A. Y. Elezzabi, Phys. Rev. A **73**, 013815 (2006).
[21] P. Dombi, P. Rácz, and B. Bódi, Laser Part. Beams **27**, 291 (2009).
[22] P. Hommelhoff, Y. Sortais, A. Aghajani-Talesh, and M. A. Kasevich, Phys. Rev. Lett. **96**, 077401 (2006).
[23] K. C. Kulander, K. J. Schafer, and J. L. Krause, in *Proceedings of the Workshop on Super Intense Laser Atom Physics (SILAP III)*, edited by B. Piraux (Plenum, New York, 1993), Vol. 316, p. 95.
[24] P. B. Corkum, Phys. Rev. Lett. **71**, 1994 (1993).
[25] M. Schenk, M. Krüger, and P. Hommelhoff, Phys. Rev. Lett. **105**, 257601 (2010).
[26] P. Eckle *et al.*, Science **322**, 1525 (2008).
[27] M. Schultze *et al.*, Science **328**, 1658 (2010).
[28] A. S. Kheifets and I. A. Ivanov, Phys. Rev. Lett. **105**, 233002 (2010).
[29] K. Klünder *et al.*, Phys. Rev. Lett. **106**, 143002 (2011).
[30] H. Raether, *Surface Plasmons on Smooth and Rough Surfaces and on Gratings* (Springer, Berlin, 1988).
[31] *Handbook of Optical Constants of Solids*, edited by E. D. Palik (Academic, San Diego, 1985).
[32] S. Kim, J. Jin, Y.-J. Kim, I.-Y. Park, Y. Kim, and S.-W. Kim, Nature (London) **453**, 757 (2008).
[33] I. Park, K. Seugchul, C. Joonhee, D. H. Lee, Y.-J. Kim, M. F. Kling, M. I. Stockman, and S.-W. Kim, Nat. Photonics **5**, 677 (2011).